Acta Polytechnica **27**(0):84–89, 2020
doi:10.14311/APP.2020.27.0084

available online at http://ojs.cvut.cz/ojs/index.php/app

DISTRIBUTION OF HYDRATION PRODUCTS IN THE MICROSTRUCTURE OF CEMENT PASTES

Michal Hlobil

Czech Academy of Sciences, Institute of Theoretical and Applied Mechanics, Prosecká 809/76, 19000 Prague, Czech Republic

correspondence: hlobil@itam.cas.cz

Abstract. This case study focuses on the quantification of the amorphous hydrate distribution in the microstructure of hardened cement paste. Microtomographic scans of the hardenend cement paste were thresholded based on histogram image analysis combined with microstructural composition obtained from CEMHYD3D hydration model, to separate unhydrated cement grains, crystalline and amorphous hydrates, and capillary pores. The observed spatial distribution of the amorphous hydrate exhibited a strong spatial gradient as the amorphous gel tended to concentrate around dissolving cement grains rather than precipitate uniformly in the available space. A comparative numerical study was carried out to highlight the effect of the spatially (non)uniform hydrate distribution on the compressive strength of the hardened cement paste.

Keywords: Cement paste, hydration products, microstructure, modelling.

1. Introduction

Upon contact with water, the clinker and gypsum grains present in Portland cement start to dissolve, releasing ions into the solution. Upon saturation, hydration products (i.e. hydrates) begin to precipitate on their surface. With progressing cement dissolution, the hydrates fully cover the grains and form dense reaction rims. These then densify with time, gradually expand into the available pore space, and eventually interconnect each other to form a solid internal network. Hydrates in Portland cement pastes consist primarily of the amorphous calcium-(aluminate)-silicate-hydrate (C-(A)-S-H) gel as well as other crystalline hydrates, namely portlandite (CH), monosulfate (AFm), ettringite (Aft), and others, depending on the mineral cement composition [1]. The amorphous C-S-H gel occupies the largest volume fraction in the hydrated cement paste microstructure, and is therefore largely responsible for the engineering properties of the material. The distribution of the amorphous gel in space depends on several factors, namely on the particle size distribution of the cement (clinker) used and consequently on its fineness, on the spacing of cement grains in the mixture governed by the water-to-cement ratio, and on the mineralogical cement composition.

The microstructure of cementitious composites can nowadays be commonly visualized with a scanning electron microscope (SEM), in particular using the backscattered electron mode (BSE), provided a suitable specimen cross-section is prepared [2, 3]. In particular, the specimen must be cut, polished and carbon/gold coated for greater viewing sharpness, which adds to a rather laborious preparation [4]. Recent developments of in the field of computed microtomography allow to analyze specimens not only without any prior surface treatment, but also allow to see into the specimen, in particular to reconstruct the whole 3D microstructure [5]. This opens the door for the characterization of volume-based characteristics of the microstructure, such as percolation or spatial distribution of phases.

Oxides	**[wt %]**	**st. dev**
CaO	65.04	0.43
SiO_2	20.60	0.25
Al_2O_3	5.60	0.24
MgO	1.47	0.10
Na_2O	0.10	0.02
K_2O	0.61	0.02
SO_3	2.31	0.07
P_2O_5	0.10	0.01
Fe_2O_3	2.49	0.06

Table 1. Chemical composition of cement ID 133 determined by EDX.

2. Materials and Methods

The cement used in this study was produced in the ASTM Cement and Concrete Reference Laboratory (NIST), USA, under the ID 133, and can be characterized as a Type I/II ordinary Portland cement with a chemical composition listed in Table 1. Gypsum was added as 5.4 % on a volume basis. The cement is ground to a Blaine fineness of about 350 m^2/kg and features a cumulative cement particle size distribution as shown in Figure 1.

Fresh cement paste was prepared by mixing conditioned distilled water and cement in a mass ratio of 0.45. Subsequently, the paste was poured into molds and kept in saturated conditions until testing.

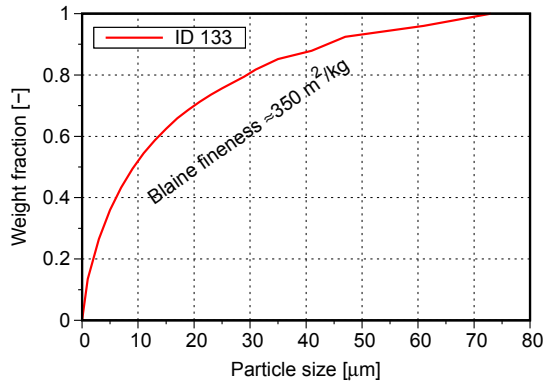

FIGURE 1. Discretized particle size distribution of cement ID 133.

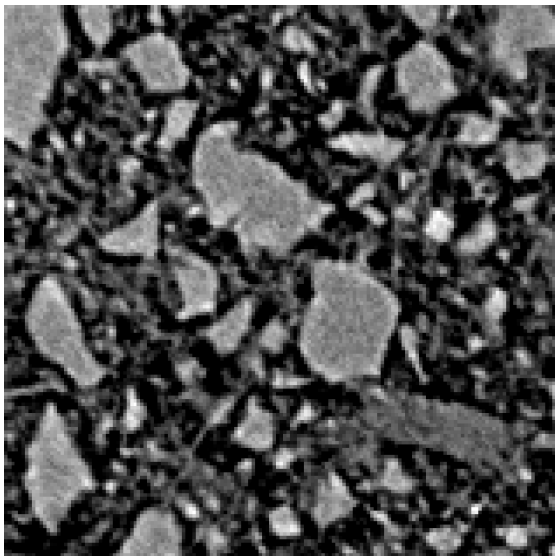

FIGURE 2. Cropped 2D slice of the tomographic data showing the microstructural features of a hardened cement paste; image size 158×158 pixels capturing an area $150 \times 150\,\mu m^2$.

2.1. TOMOGRAPHIC SCANNING OF HARDENED CEMENT PASTE

Paste specimens were demolded and scanned using a microtomograph at the European Synchrotron Radiation Facility near Grenoble, France, to obtain a three dimensional reconstruction of the cement paste microstructure at selected times. The size of the scanned volume is $1024 \times 1024 \times 512$ volume elements (voxels) with a resolution of 0.95 µm/voxel which provides an effective microstructural volume of $972 \times 972 \times 486\,\mu m^3$. The signal from the tomograph is converted into a greyscale monochrome image with color intensities proportional to the atomic number of the element encountered in the particular voxel, ranging from full black to bright white similar to the traditional SEM/BSE imaging. The 3D tomographic image captures the full microstructural features, namely the volumetric distribution of the individual material phases. Slicing the full 3D image into individual slices allows to directly visually compare the microstructure with the traditional 2D greyscale SEM/BSE images. In particular, clinker minerals and gypsum appear as bright areas which are embedded into a mid-tone grey bulk matrix consisting from a mixture of hydration products, and lastly dark grey-to-black areas correspond to capillary porosity, see Figure 2. Arbitrary segmentation of material phases from the 2D image slices is not straightforward since the 3D volume generally contains a non-negligible noise, and the distinction between hydration products and capillary porosity is challenging.

2.2. MODELING OF MICROSTRUCTURAL DEVELOPMENT

Since a quantitative microstructural analysis of the investigated hardened cement paste was not available, a simulation of the cement hydration and microstructure development was carried out using the CEMHYD3D software package developed by D. Bentz at NIST, USA [6]. In its third revision [7], CEMHYD3D attempts to reconstruct the microstructure of the investigated system by generating a 3D representation of cement particles in water, while matching the particle size distribution of the real cement along with the individual phase volume and area fractions. Periodic boundary conditions are respected during the generation of the 3D volume containing cement particles to omit the local segregation phenomena related to the wall-effect, e.g. near the outer specimen surface, or near the aggregates where ITZ forms [8]. The model accounts for the chemical reactions of the major cement minerals (alite, belite, aluminate, and ferite phases) along with calcium sulfate phases (an-/hemi-/di-hydrate). Implemented chemical reactions follow the described stoichiometry [9]. Computationally, the hydration reactions are implemented as a series of cellular automata-like rules, describing in repeated cycles the dissolution, diffusion, and interaction of diffusing species with clinker and gypsum particles. A posteriori, calibration of hydration kinetics is necessary for mapping the calculated results to real time. This is achieved by fitting the calculated results of the heat evolution into a parabolic dispersion model via

$$\text{time} = t_0 + \beta\,\text{cycle}^2, \tag{1}$$

where t_0 stands for the induction time and β is a fitting parameter, which has to be calibrated from experiments. For the present cement ID 133 studied, $t_0 = 0$ as the induction period is implicitly accounted for since the second version of this hydration model [10] by adjusting the early-dissolution probabilities for all clinker phases, which are made proportional to the square of the amount of C-S-H produced, and $\beta = 0.0003$ as identified from isocalorimetric measurements carried out in NIST.

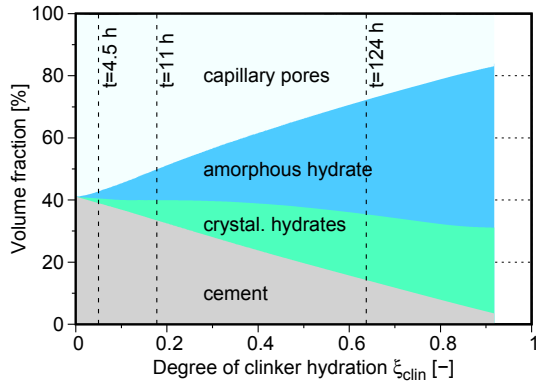

Figure 3. The volume fraction evolution of microstructural phases in cement ID 133, cured at 20 °C in saturated conditions, as simulated by CEMHYD3D.

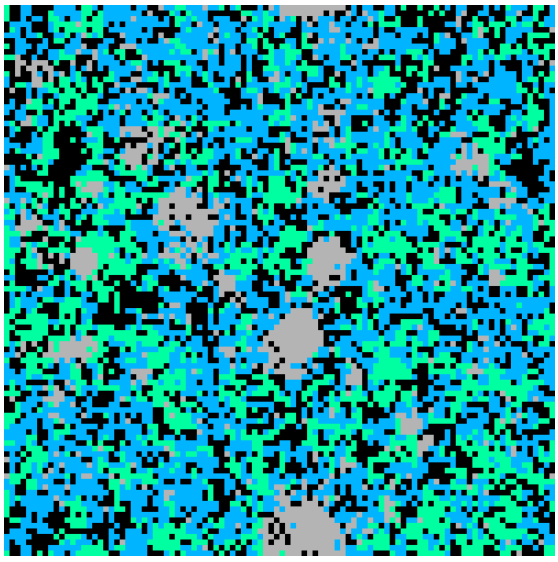

Figure 4. Partially hydrated artificial microstructure from CEMHYD3D; one slice showing a cross-section 100 × 100 µm with a resolution 1 pixel (voxel)=1 µm; color map corresponds to Figure 3.

3. Results

The microstructural evolution as quantified by simulating the hydration of an RVE of cement paste with a side equal to 100 µm using CEMHYD3D is shown in Figure 3. To simplify the microstructural characterization, all unhydrated clinker phases together with all calcium sulfate forms (including secondary gypsum formed) are merged together into the phase labeled as "cement". Similar simplification was done also for crystalline hydrates which include portlandite, ettringite, monosulfate, and iron hydroxide. The amorphous hydrate then consists of the calcium silicate and calcium aluminate hydrates. A single 2D slice of the modeled microstructure from CEMHYD3D is then shown in Figure 4 with a color map matching Figure 3.

Combining histogram image analysis with known (calculated) volume fractions of material phases opens door for accurate thresholding of the tomographic

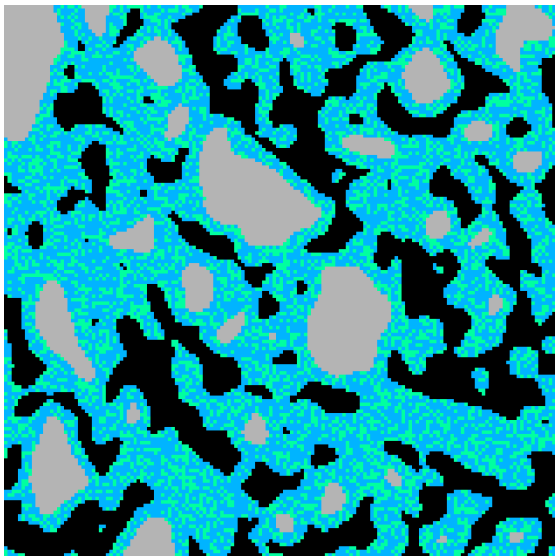

Figure 5. Thresholded 2D slice of the tomographic data separating cement (clinker+calcium sulfate phases), amorphous and crystalline hydrates, and capillary porosity; image size 158 × 158 pixels capturing an area 150 × 150 µm^2; color map corresponds to Figure 3.

slices, as described next. First, a 2D slice from the tomographic data is extracted and cropped to 158 × 158 pixels capturing an area of 150 × 150 µm to reduce computational time for analysis and yet cover a sufficiently large area for a representative analysis. Since the raw tomographic data contains noise, a suitable smoothing image filter is applied to reduce the image noise. Subsequently, a histogram of the cropped image is produced, quantifying the amount of pixels of a given grey shade in 8 bit color depth, i.e. 255 colors, ranging from 0 (representing black) to 255 (white). Converting the histogram into its cumulative form, and normalizing it with respect to the total amount of pixels in the image allows to keep the abscissa values and renumber the ordinate from 0 to 1. In such form, the cumulative histogram can be used to identify two threshold values for porosity and cement particles by comparing the calculated volume fractions from CEMHYD3D with the ordinate values, pointing to the sought threshold values on the abscissa. The greyscale values lying in between these limits are attributed to the hydration products.

Separation of the hydrate phase into the crystalline and amorphous parts is not possible using histogram analysis, since the phase contrast manifesting as similar grey shade is too low. However, the formation of crystalline hydrates within the microstructure is random as they tend to form both on the surface of cement particles as well as nucleate within the amorphous hydrate [11] Consequently, the crystalline hydrates were randomly distributed within the hydration products following their volume fraction, see Figure 5 for final result.

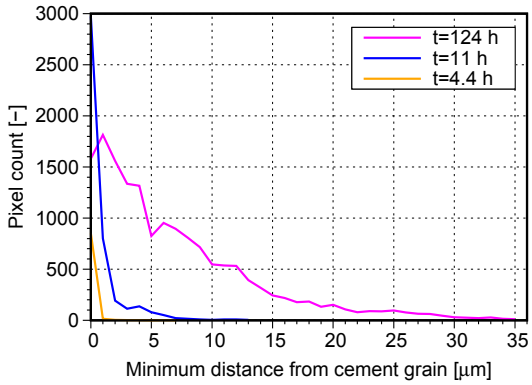

FIGURE 6. Quantification of the spatial distribution of amorphous hydrates as a function of the minimum distance from the cement grain.

3.1. SPATIAL DISTRIBUTION OF AMORPHOUS HYDRATES

Quantification of the spatial distribution of the amorphous hydrate gel from the thresholded tomographic image is performed by measuring the distance between the given amorphous hydrate pixel and the closest cement particle. Counting such minimum distances for all hydrate pixels in the image and binning the results shows a rather strongly non-uniform hydrate distribution in the cement paste microstructure, see Figure 6. In the early stages of hydration (4.5 and 11 hours), the amorphous hydrates form dominantly around cement grains which can be seen as the distance from the grain is rather short, i.e. only single units of micrometers. With progressing hydration, cement grains dissolve and create additional space for new hydrates to form. However, even then the hydrates tend to precipitate in rings, minimizing the distance to the nearest cement grain, and do not precipitate randomly in space.

3.2. PREDICTION OF CEMENT PASTE COMPRESSIVE STRENGTH

Local spatial distribution of hydration products directly affects the macroscopic mechanical properties of cement paste, in particular the compressive strength. Two case studies will be considered to show the impact of the hydrate distribution, namely i) the hydrate density distribution exhibiting a strong spatial gradient as observed in thresholded micrographs, see Figure 5, and ii) an uniform hydrate distribution. In both cases, the cement grain locations as well as volume fractions of all phases remain identical. The only difference stems from the fact, that in the second case, the hydrates are smeared uniformly throughout the microstructure, which effectively changes the capillary pore size system, compare Figures 5 and 7.

A micromechanical model based on finite element homogenization is formulated for both cases in such a way that the finite element mesh is generated over the thresholded bitmap micrograph using quadrilateral elements in place of image pixels. Local mechanical properties of the identified phases, e.g. of clinker,

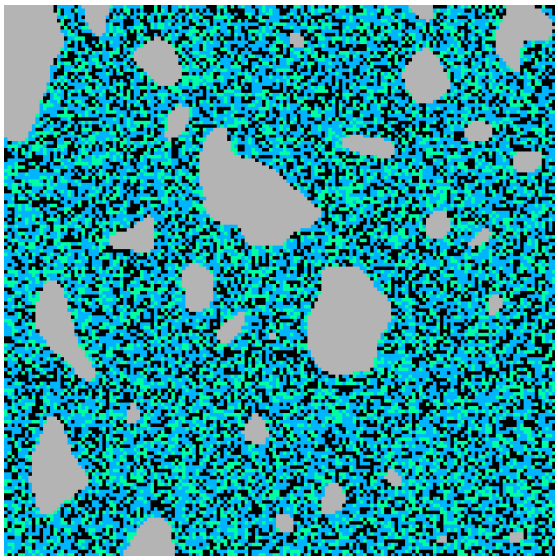

FIGURE 7. Artificially created microstructure based on Figure 5, featuring an enforced uniform distribution of hydrates in space; image size 158×158 pixels capturing an area of 150 × 150 µm^2; color map corresponds to Figure 3.

Phase	E [GPa]	ν [–]	f_t [MPa]	G_f [J/m^2]	**ref**
clinker	139.9	0.30	–	–	[13]
amorph. hyd.	24.4	0.24	264.1	4.4	[12]
crystal. hyd.	42.3	0.32	–	–	[14]
porosity	0.001	0.49	–	–	[15]

TABLE 2. Material properties obtained from nanoindentation.

of amorphous and crystalline hydration products are obtained by nanoindentation measurements [12], see Table 2.

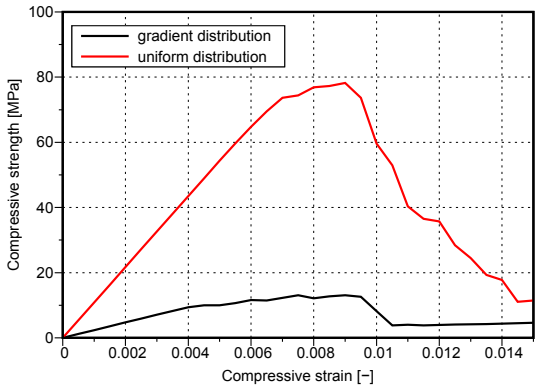

FIGURE 8. Results of compressive strength simulation for both hydrate spatial distributions (gradient and uniform) for virtual microstructures of cement ID 133 at 124 hrs.

Two distinct material models are assigned to the individual phases. A simple linear elastic constitutive behavior is used for cement, crystalline hydrates, and

porosity, whereas the amorphous hydrates are modeled using a nonlinear fracture mechanics approach combined with an isotropic damage model for tensile failure, originally described in [16]. The virtual model of the microstructure features periodic boundary conditions in the vertical direction along with supported nodes to prevent rigid body translation and rotation. The problem is solved in the plane stress domain using a nonlinear static analysis carried out with the Newton-Raphson iterative solver by applying a predefined eigenstrain load increment until failure.

Results of the microstructural simulation are shown in Figure 8. The microstructure based on the thresholded tomographic data exhibits a peak compressive strength of 13.7 MPa, whereas the virtual microstructure exhibiting an uniform distribution of hydrates fails at 78.2 MPa. Such an increase of 470% was achieved by changing the hydrate spatial density distribution while keeping the volume fractions of all phases identical.

4. Conclusions

Combining state-of-the-art microtomography to obtain a 3D microstructure with the quantification of volume phases using a hydration model CEMHYD3D allowed to view, threshold and separate the cement grains, crystalline and amorphous products, and capillary pores in a representative volume of hardended cement paste with initial water-to-cement ratio of 0.45. Focusing on the amorphous hydrate phase, its distribution was measured by determining the minimum distances of each hydrate pixel to the closest cement grain. Results of this study indicate a non-uniform distribution with a strong gradient in space. In the early stage of hydration, the hydrates precipitate dominantly around cement grains. With ongoing hydration the distances between cement grains increase as these dissolve, however even then the hydrates tend to minimize the necessary distance and precipitate in rings rather than randomly in space.

Numerical modeling showed that enforcing an uniform hydrate distribution on the same microstructure (*same* by means of identical volume fractions of all phases and identical placement of unhydrated cement grains) resulted in a significant increase of compressive strength. This stems from the fact that the uniform hydrate distribution resulted in an alternation of the capillary pore shape and an effective pore size decrease, which consequently manifested as an increase of hardened cement paste compressive strength.

Acknowledgements

The author gratefully acknowledges support from the Czech Science Foundation project 19-25163Y.

References

[1] P. Termkhajornkit, Q. H. Vu, R. Barbarulo, et al. Dependence of compressive strength on phase assemblage in cement pastes: Beyond gel–space ratio - Experimental evidence and micromechanical modeling. *Cement and Concrete Research* **56**:1–11, 2014. doi:10.1016/j.cemconres.2013.10.007.

[2] S. Diamond. The microstructure of cement paste and concrete - a visual primer. *Cement and Concrete Composites* **26**(8):919–933, 2004. doi:10.1016/j.cemconcomp.2004.02.028.

[3] K. Scrivener. Backscattered electron imaging of cementitious microstructures: understanding and quantification. *Cement and Concrete Composites* **26**(8):935–945, 2004. doi:10.1016/j.cemconcomp.2004.02.029.

[4] K. L. Scrivener, R. Snellings, B. Lothenbach. *A Practical Guide to Microstructural Analysis of Cementitious Materials*. CRC Press, 2016.

[5] E. Gallucci, K. Scrivener, A. Groso, et al. 3D experimental investigation of the microstructure of cement pastes using synchrotron X-ray microtomography (μCT). *Cement and Concrete Research* 2007.

[6] D. P. Bentz. A three-dimensional cement hydration and microstructure program. I. Hydration rate, heat of hydration and chemical shrinkage. Tech. rep., NIST Building and Fire Research Laboratory, Gaithersburg, Maryland, 1995.

[7] D. P. Bentz. CEMHYD3D: A Three-Dimensional Cement Hydration and Microstructure Development Modeling Package. Version 3.0. Tech. rep., NIST Building and Fire Research Laboratory, Gaithersburg, Maryland, 2005.

[8] K. L. Scrivener, A. K. Crumbie, P. Laugesen. The Interfacial Transition Zone (ITZ) Between Cement Paste and Aggregate in Concrete. *Interface Science* **12**(4):411–421, 2004.

[9] H. F. W. Taylor. *Cement chemistry*. Thomas Telford Publishing, 2nd edn., 1997.

[10] D. P. Bentz. CEMHYD3D: A Three-Dimensional Cement Hydration and Microstructure Development Modeling Package. Version 2.0. Tech. rep., NIST Building and Fire Research Laboratory, Gaithersburg, Maryland, 2000.

[11] F.-J. Ulm, M. Vandamme, H. Jennings, et al. Does microstructure matter for statistical nanoindentation techniques? *Cement and Concrete Composites* **32**(1):92–99, 2010.

[12] J. Němeček, V. Králík, V. Šmilauer, et al. Tensile strength of hydrated cement paste phases assessed by micro-bending tests and nanoindentation. *Cement and Concrete Composites* **73**:164–173, 2016. doi:10.1016/j.cemconcomp.2016.07.010.

[13] K. Velez, S. Maximilien, D. Damidot, et al. Determination by nanoindentation of elastic modulus and hardness of pure constituents of Portland cement clinker. *Cement and Concrete Research* **31**(4):555–561, 2001. doi:10.1016/S0008-8846(00)00505-6.

[14] C.-J. Haecker, E. J. Garboczi, J. W. Bullard, et al. Modeling the linear elastic properties of Portland cement paste. *Cement and Concrete Research* **35**(10):1948–1960, 2005. doi:10.1016/j.cemconres.2005.05.001.

[15] V. Šmilauer, Z. Bittnar. Microstructure-based micromechanical prediction of elastic properties in hydrating cement paste. *Cement and Concrete Research* **36**(9):1708–1718, 2006. DOI:10.1016/j.cemconres.2006.05.014.

[16] M. Hlobil, V. Šmilauer, G. Chanvillard. Micromechanical multiscale fracture model for compressive strength of blended cement pastes. *Cement and Concrete Research* **83**:188–202, 2016.